6.1. Materials.

Miminum essential medium(MEM), Fetal Bovine serum(FBS),Antibiotic antimycotic solution 100x, Culture flask for adherent cell lines, well plates, MTT (3-(4,5-Dimethylthiazol-2-yl)-2,5-Diphenyltetrazolium Bromide), dimethyl sulphoxide (biochemistry grade), Fluorescein isothiocyanate (FITC), DAPI (4′,6-diamidino-2-phenylindole) and Paraformaldehyde were procured from HiMedia, India. mCherry-Mito-7, Lipofectamine® 3000, Propidium Iodide (#P1304MP) were procured from Thermofisher, USA. Pro-long media, TMRM stain (Tetramethylrhodamine, Methyl Ester, Perchlorate) and ATP determination kit were procured from Molecular Probes, Life Technologies, Canada. Isopropyl alcohol and sodium hydroxide AR grade was procured from Rankem, India. Triton X100 was procured from Sigma Aldrich, USA. All buffers were prepared in house using filtered double distilled water.

6.1. Procurement and subculture of cell lines.

The U87MG glioblastoma cell lines were procured from National centre for cell sciences, Pune, Maharashtra, India. The cell line was cultured in vented flasks for adherent cell lines of 25cm^2 area aseptically. The culture medium was composed of MEM with 10% Fetal bovine serum and 0.1% antibiotic antimycotic solution. The subculturing was done as per ATCC guidelines in the ratio of 1:2 and media change was given 2-3 times per week. The cell line flasks were examined periodically to monitor the growth of cells and to check for contamination as shown in figure 6.1.The cultured U87MG cell lines were used in all the studies.

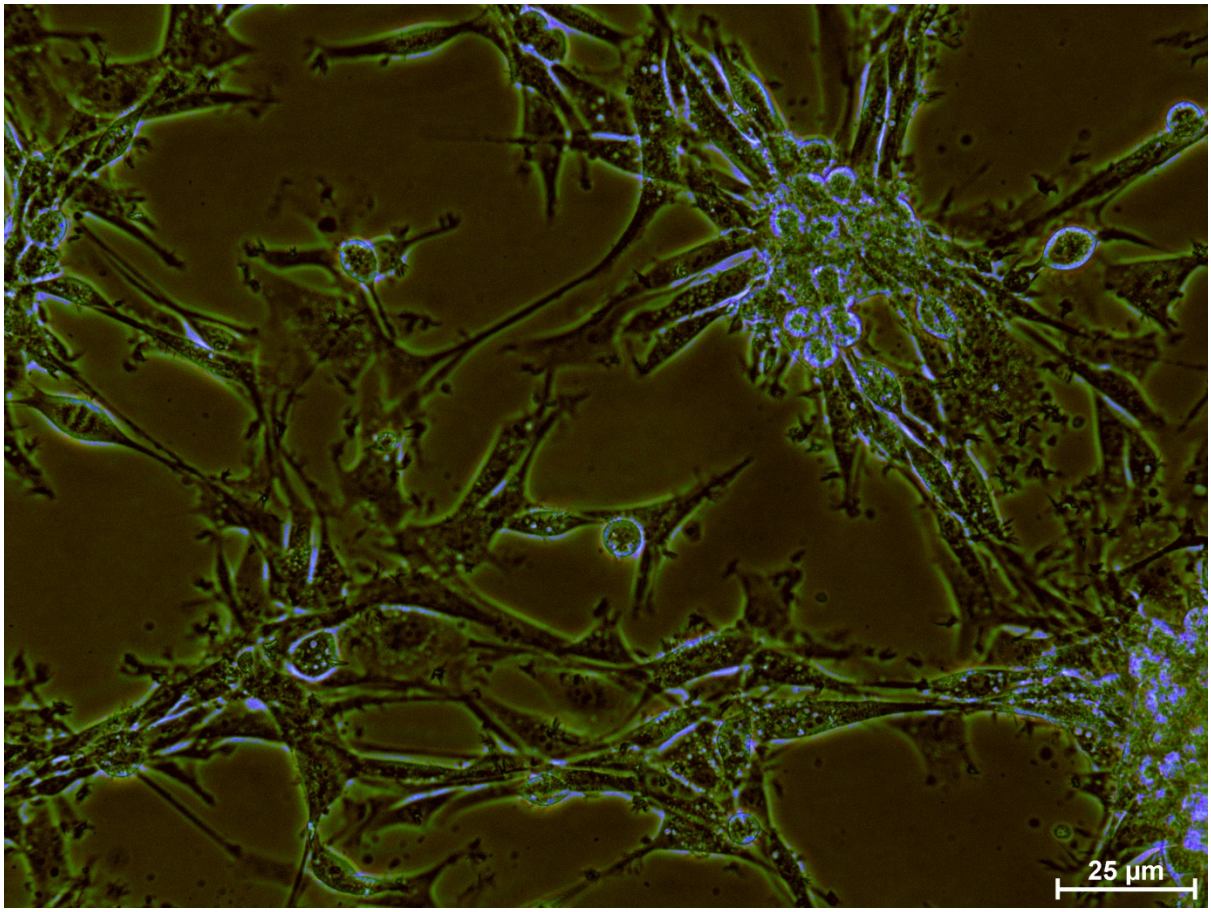

Figure 6.1:U87MG glioblastoma cell lines cultured aseptically.

6.2. In vitro cytotoxicity (MTT assay).

For the assay, U87MG glioblastoma cell lines were cultured in sterile 96 well plates at counts of 25000 cells /well and were given incubation for 24 hours with replacement of culture media after adherence of cells. The cell line was treated with 200µl of concentrations of 20-100µg/ml of the following series of the formulation components in triplicate.

a) Drug (lenalidomide)
b) Gd-doped iron oxide nanoparticles (metallic core).
c) Drug coated metallic core.
d) Theranostic nanoparticles.

The aliquots for the components were prepared in culture media aseptically before treatment. After 24 hours of treatment the contents of each well was removed using a sterile pipette and 100µl of 1mg/ml of MTT dye in sterile PBS was added to each well and incubated in dark for 3 hours.

The purple formazan crystals formed during the incubation period were dissolved using 200µl of dimethyl sulphoxide .The absorbance of the wells was taken along with the blank at 570nm using plate reader (Biotek synergy, HTX,USA) (1-3).

6.3. Cell migration assay (Scratch assay).

The U87MG cells were cultured in sterile 6 well plates till the confluency reached 90-95%. The well plates were examined daily to check the cell growth using an inverted microscope (Nikon, Eclipse, Ti-2, Japan).The scratch was made in the middle of each well plate using a sterile 200µl microtip. All wells were treated with 200µl of the theranostic nanoparticles with drug concentration of 20-100µg/ml except one well which was kept as control. The well plates were observed under microscope at the time intervals of 24 and 48 hours (4, 5).

6.4. Confocal microscopy.

The localization of nanoparticles intracellularly was observed visually by confocal microscopy. The U87MG cells were seeded at the density of $1.5x10^5$ cells per well in a 24 well plate. The glioblastoma cell lines were transfected with mCherry-Mito-7 using Lipofectamine® 3000.

After 24 hours of transfection the cells were exposed to FITC tagged theranostic nanoparticles at concentration of 0.8mg/ml for a period of 4 hours. The tagging of theranostic nanoparticles was done during the assembly step where the PEI-FA-TPP solution was incubated FITC such that the resultant concentration of the FITC was 2µg/ml and pH was adjusted to 11 using 0.01 M NaOH. The mixture was kept in dark for 24 hours and dialysed for 4 hours to remove unbound FITC after which the FITC tagged PEI-FA-TPP was used to coat the drug coated core (6).

The slides and coverslips were rinsed with phosphate buffer saline and treated with 4% paraformaldehyde for 30 minutes followed by washing with buffer and nuclear staining with DAPI after which mounting in pro-long media was accomplished. The examination was done with confocal microscope, Zeiss, LSM-710, Germany using appropriate excitation sources and filters (7, 8).

6.5. Mitochondrial membrane potential (TMRM) and ATP levels.

In a 96 well plate, the U87MG cells were seeded at the density of 10000 cells/well. The cells were treated with 20-100µg/ml of drug and drug equivalent theranostic nanoparticles. The mitochondrial potential was determined using TMRM stain for 15 min followed by quantification of fluorescence at 510/570–600 by plate reader Biotek synergy, HTX,USA (9).

For determination of ATP levels the glioblastoma cell lines were seeded in density of 50000 cells/well. The cells were treated with 20-100µg/ml of drug and drug equivalent theranostic nanoparticles. The ATP levels were estimated using ATP determination kit in which 1:10 dilution of cell lysate was done in ATP master mix. The luminescence intensity was measured using Multimode Microplate Reader, Biotek synergy, HTX, USA (10).

6.6. PI staining.

The U87MG cells were seeded in 10000 cells /well in a 96 well plate followed by treatment of 20-100µg/ml of drug and drug equivalent theranostic nanoparticles. After the treatment, the cells were washed with PBS and stained with10 µM Propidium Iodide solution for 30 min followed by washing with DPBS. The florescence was measured at excitation wavelength 530nm and emission of 590 nm using Biotek synergy, HTX,USA (11)

6.7. Mucosal toxicity study.

The intact nasal mucosa of goat was procured from local slaughter house and divided into three equal sections. In a 6 well plate, one section was treated with isopropyl alcohol (positive control), second section was treated with phosphate buffer saline pH 7.4 (negative control) and the third was treated with 1 ml theranostic nanoparticle dispersion (equivalent to 500µg drug) for 1 hour. After the exposure period all the sections were rinsed with double distilled water in the well plate and preserved in formalin solution till sectioning was done with microtome with staining of hematoxylin-eosin for microscopic examination (12, 13).

6.8. Hemolytic toxicity.

The blood was sourced from tail veins of rats which was collected in EDTA coated tubes to prevent coagulation. The RBCs were separated from plasma by centrifugation at 1000 rpm for 10 minutes. The RBCs were separated from the plasma and washed with phosphate buffer saline pH 7.4 and redispersed in phosphate buffer saline for further use.

The diluted RBC suspension was treated with theranostic nanoparticles such that the final concentration of drug in dilution would be 1-500µg/ml. The positive control was prepared by mixing the RBC dispersion with 2% v/v triton X100 surfactant and RBCs diluted with phosphate buffer saline were kept as negative controls. After the treatments, the RBCs were separated from the medium and clear supernatant obtained after centrifugation at 10000 rpm for 10 minutes was analysed at 541 nm using UV spectrophotometer, UV-1800, Shimadzu, Japan. The % Hemolysis was calculated using the following equation (14, 15).

$$\%Hemolysis = Abs\,(sample) - Abs\,(-ve\ ctrl) \,/\, Abs\,(+ve\ ctrl) - Abs\,(-ve\ ctrl) \times 100$$

6.9. Results and discussions.

6.9.1. MTT assay.

The MTT (3-(4,5-dimethylthiazol-2-yl)-2,5-diphenyltetrazolium bromide) assay is used to assess the cytotoxicity of a drug or formulation and is based on the principle of conversion of MTT dye to formazan by the enzymatic reduction in mitochondria as shown in figure 6.2 . The MTT dye is a water soluble dye which can cross the cell membranes into mitochondria but the formazan dye formed by the mitochondrial metabolism is insoluble and is solubilised using solvents like DMSO or ethanol following by the measurement of absorbance at 570nm corresponding to the cell viability (16).

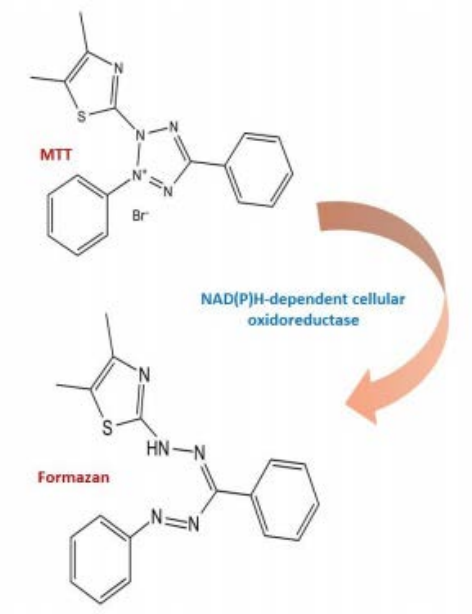

Figure 6.2: Principle of MTT assay.

The results of MTT assay are shown in figure 6.3. It can be seen that as compared to control all the other components like the drug lenalidomide, metallic core, drug coated core and final formulation of theranostic nanoparticles exhibit cytotoxicity. There exists a linear relationship in all the cases as with the increase in concentration of the drug the cell viability decreased. This observation is same for the metallic core, drug coated core and final formulation of theranostic nanoparticles.

The theranostic nanoparticles exhibited the highest cytotoxicity as the cell viability is lower than 50% for the lowest concentration of 20µg/ml of drug in the formulation while the highest concentration of 100µg/ml of drug in theranostic nanoparticles showed viability less than 10 % which indicated that the formulation of theranostic nanoparticles enhanced the cytotoxicity of the drug. The IC_{50} value calculated theoretically which was found to be 1.85µg/ml from the regression equation obtained by plotting % cell viability against the concentration of drug in the formulation. The low IC_{50} value highlighted the cytotoxic behaviour of the formulation as lower the value, the greater is the cytotoxic potential of the substance under examination (17).

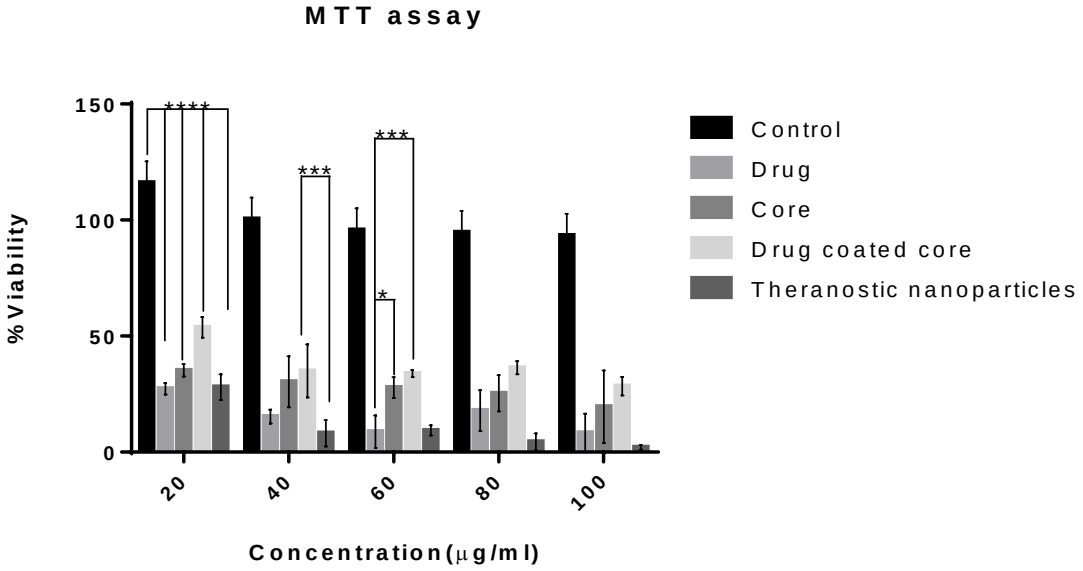

Figure 6.3: Results of MTT assay (n=3).

ANOVA analysis(α=0.05), P ≤ 0.05(*), P ≤ 0.01(**),P ≤ 0.001(***), P ≤ 0.0001(****).

6.9.2. Cell migration assay (scratch assay).

In case of cancerous cells, cell migration is a critical phenomenon related to the survival and proliferation of cells. The cancerous cells disintegrate from primary tumours and invade other organs through the circulatory system by the process known as metastasis. In case of the scratch assay, the ability of the drug or formulation to inhibit the cell migration of metastasis is evaluated qualitatively (18). As shown in figure 6.4, the observations made at initial stage and at 48 hours show the ability of the theranostic nanoparticles to arrest the metastasis.

In case of the control group after period 48 hours post, scratch there was migration of U87MG cells in the scratch area followed by their proliferation. The theranostic nanoparticles containing 20µg/ml of drug which is the lowest concentration showed reduction in no of cells migrating to the scratched area as compared to control while the well treated with 100g/ml of drug containing theranostic nanoparticles showed cell death and inhibition of migration of the cells towards the scratched area. Thus it can be concluded that higher the concentration of the drug in theranostic nanoparticles more is the inhibition of metastasis (19, 20).

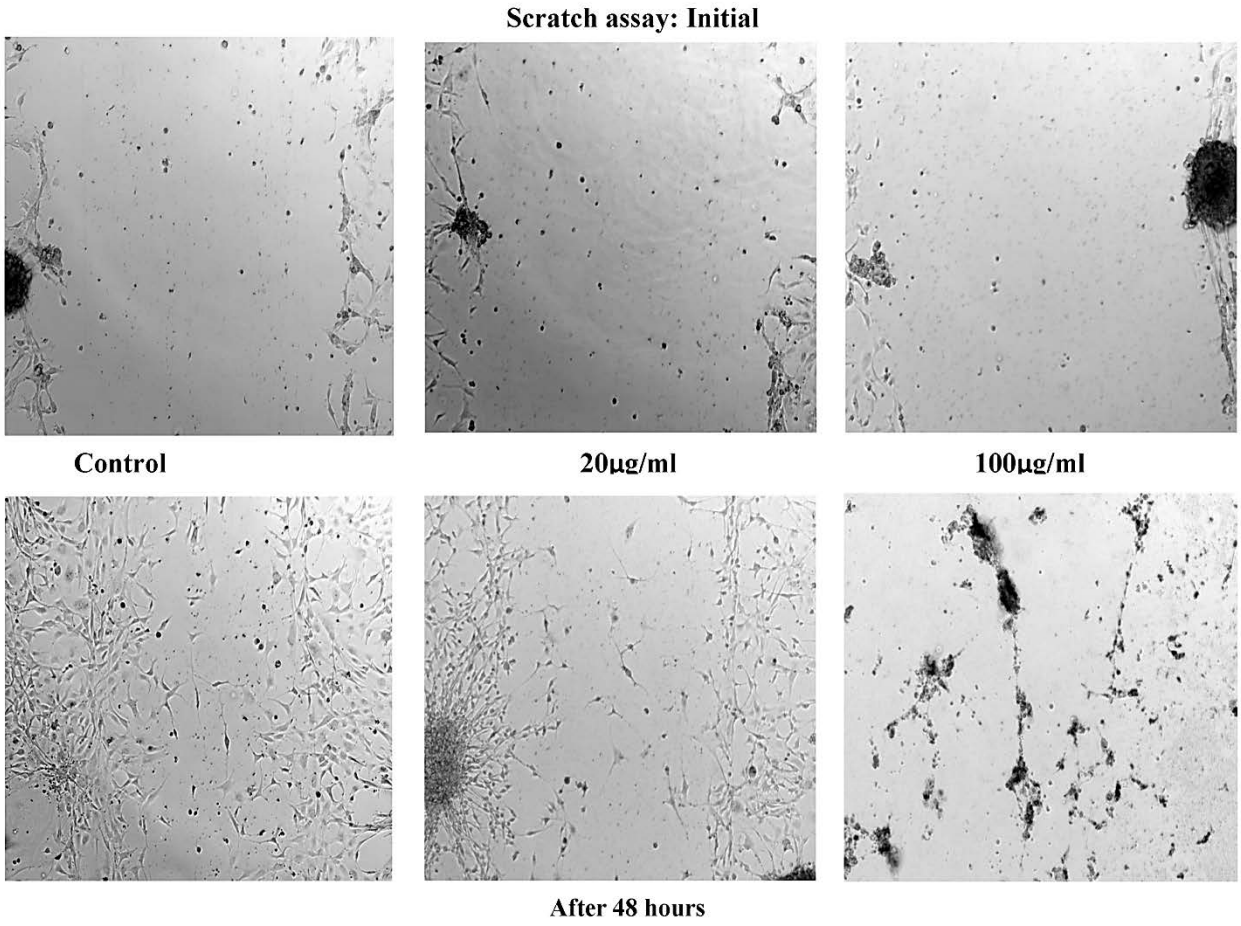

Figure 6.4: Observations of scratch assay at initial phase and after 48 hours.

6.9.3. Confocal microscopy.

The confocal microscopy revealed the internalization of the FITC labelled theranostic nanoparticles (green) into the mitochondrial vicinity (red) as observed in overlay of figure 6.5.The internalization of the theranostic nanoparticles can be attributed to the secondary PEI coat modified with folic acid and Triphenylphosphonium which aided the cell and mitochondrial uptake of nanoparticles respectively. The cancerous cells have overexpressed folate receptors which bind with folic acid ligand present on the modified PEI followed by its internalization (21). The cationic nature of the PEI and Triphenylphosphonium aid in targeting mitochondria(22). The 3-D visualization generated by the ZEISS ZEN black edition 3.0 SR software in figure 6.6 also shows the same results. The mitochondrial targeting can be useful for delivery of various molecules to the mitochondria and can also assist in amplification of cytotoxicity through disruption of mitochondrial function by various mechanisms which will enhance the treatment of cancer through organelle targeting (tertiary level of drug targeting). The effect of localization of theranostic nanoparticles can also be seen in assays like MTT, TMRM and ATP levels where the disruption of the mitochondrial function is determined quantitatively (23, 24).

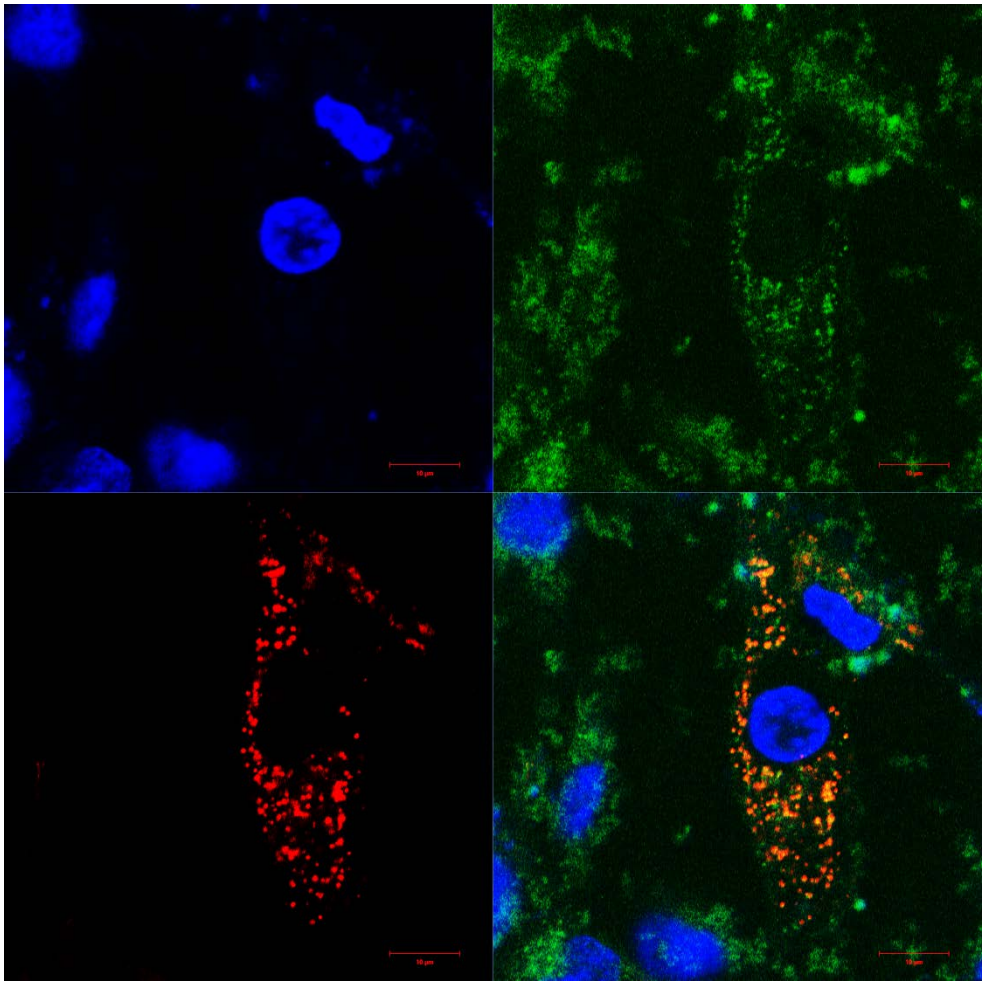

Figure 6.5: Confocal image of U87MG cell lines with nucleus (blue), mitochondria (red) and FITC tagged theranostic nanoparticles (green) and their overlay.

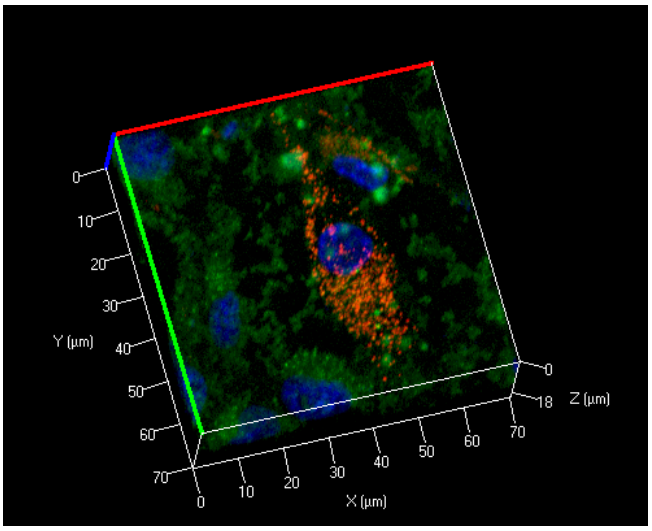

Figure 6.6: 3-D visualization of confocal microscopy of U87MG cell lines with mitochondrial internalization of theranostic nanoparticles.

6.9.4. Mitochondrial membrane potential (TMRM) and ATP levels.

The mitochondrial membrane potential and the ATP levels are mitochondrial function assays which are shown in figure 6.7 and 6.8. There was a similar concentration dependant effect observed in both the cases. In case of mitochondrial membrane potential, the free drug showed decrease in mitochondrial potential for the concentration range of 40-100µg/ml while the formulation of theranostic nanoparticles showed no change in membrane potential for the drug concentrations of 20 and 40 µg/ml but on further increase in concentration showed remarkable decrease in membrane potential as compared to control. In case of ATP level assay, a non-linear relationship has been observed. For the free drug, the ATP levels increase with increase in concentration from 20-60µg/ml but on further increase in concentration caused drastic reduction of ATP levels which was similar to that exhibited by the theranostic nanoparticles. The changes in mitochondrial membrane potential and ATP levels are indicators of mitochondrial stress and can be caused by the accumulation of drug and nanoparticles inside the mitochondria which can be seen in confocal microscopy and can further lead to apoptosis or cell death which is confirmed by the low viability from the results of MTT assay which depends on the mitochondrial metabolism in conversion of MTT to formazan (25-27).

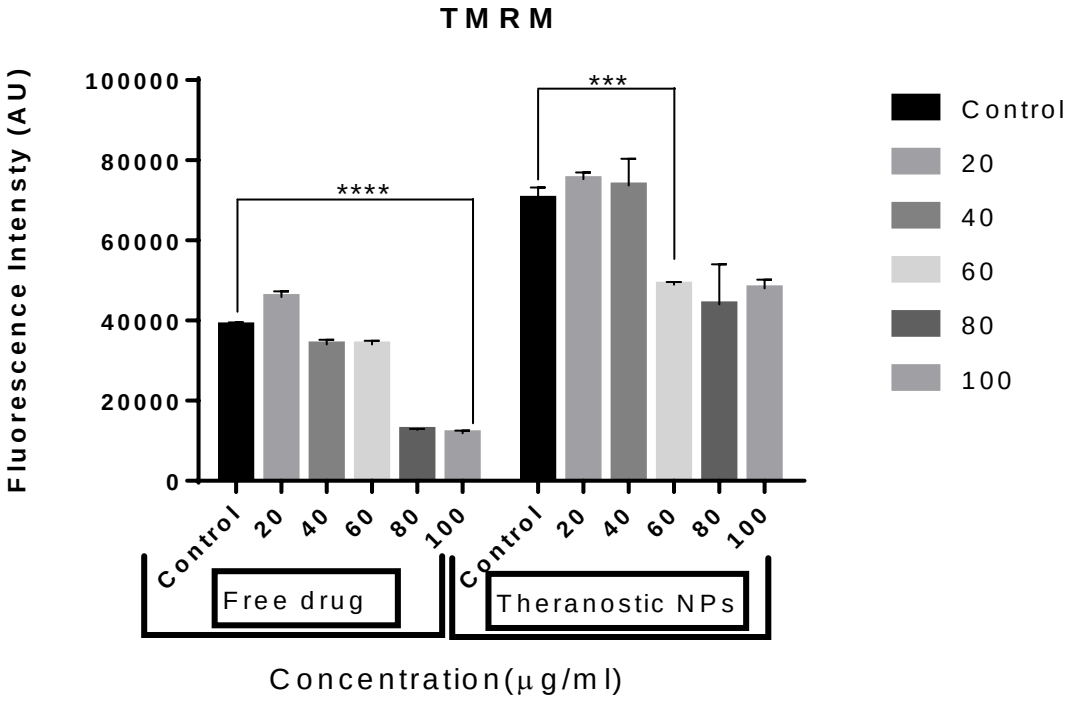

Figure 6.7: Results of mitochondrial membrane potential assay (n=3).

ANOVA analysis(α=0.05), P ≤ 0.05(*), P ≤ 0.01(**),P ≤ 0.001(***), P ≤ 0.0001(****).

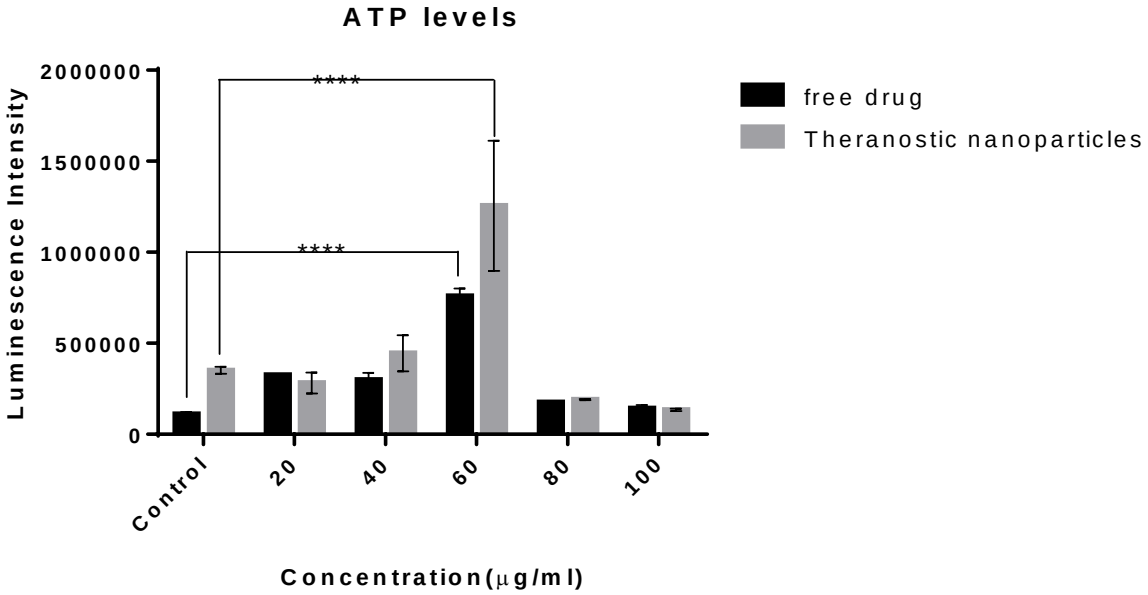

Figure 6.8: Results of ATP level assay (n=3).

ANOVA analysis(α=0.05), P ≤ 0.05(*), P ≤ 0.01(**),P ≤ 0.001(***), P ≤ 0.0001(****).

6.9.5. PI staining.

The propidium iodide is a dye which cannot permeate the live cells but can permeate non-viable or dead cells. The dye binds to the nucleic acids present in non-viable cells and exhibits florescence. As shown in figure 6.9, the free drug does not show any significant change in florescent intensity with increase in the concentration but the formulation of theranostic nanoparticles have higher florescent intensities than control and drug series which indicated that the cells have undergone apoptosis or are non-viable. The theranostic nanoparticles showed 4.7 times higher florescence than the control indicating the cytotoxicity of the formulation (28).

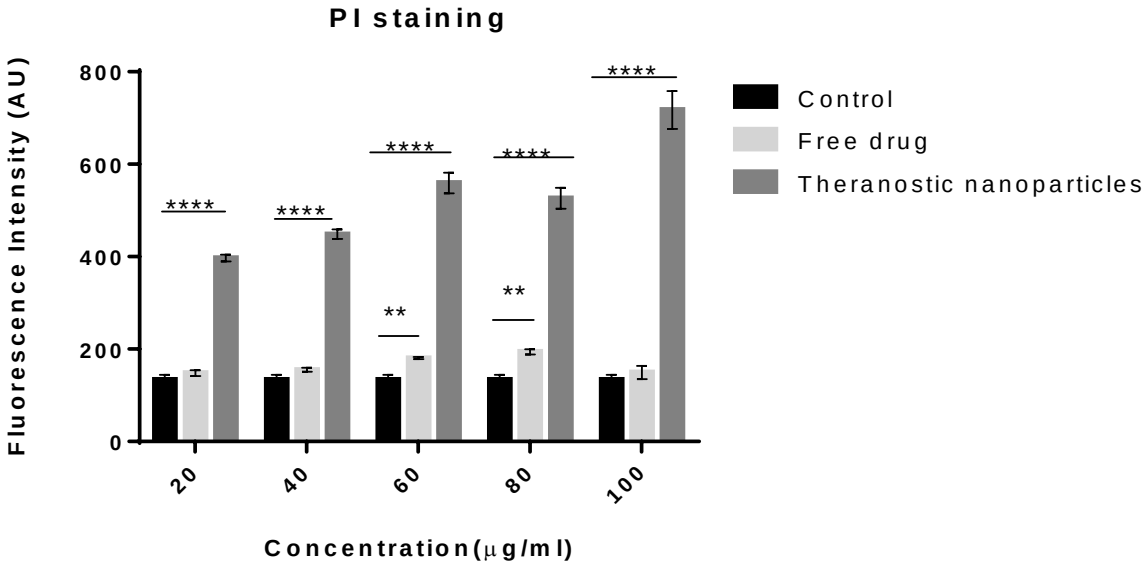

Figure 6.9: Results of PI staining (n=3).

ANOVA analysis(α=0.05), P ≤ 0.05(*), P ≤ 0.01(**),P ≤ 0.001(***), P ≤ 0.0001(****).

6.9.6. Mucosal toxicity study.

As observed microscopically from figure 6.10, the positive control shows signs of toxicity in terms of the disruption of the nasal mucosa and the fenestrations as isopropyl alcohol is a toxicity inducing solvent. The negative control shows no signs of toxicity as the mucosa appears intact and has fewer fenestrations.

The formulation appears to show minimal toxicity as compared to positive control as there are no major fenestrations produced by the formulation and the nasal mucosa appears intact as compared to the positive control (29, 30).

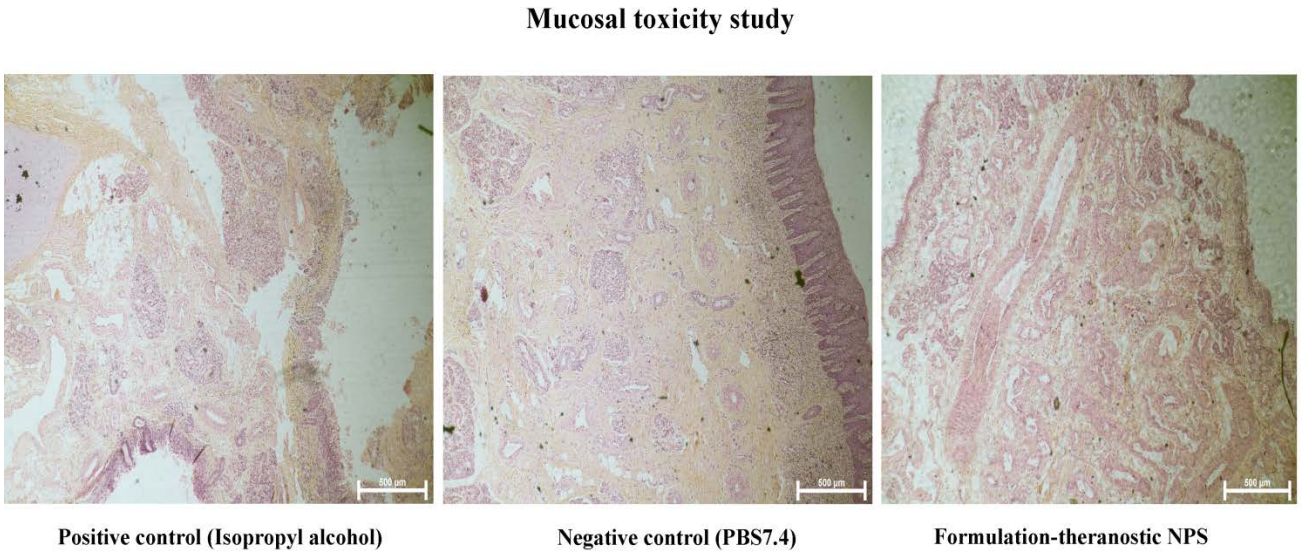

Figure 6.10: Histological observations of mucosal toxicity study.

6.9.7. Hemolytic toxicity.

The morphology of the red blood cells can be observed from figure 6.11. The positive controls showed hemolysis while the normal biconcave round morphology of RBCs was seen in case of negative control. The highest concentration of drug equivalent formulation of theranostic nanoparticles of 500ug/ml does not show any signs of toxicity in the qualitative examination. In case of quantitative analysis shown in figure 6.12, theranostic nanoparticles showed increase in hemolysis with increase in concentration of drug although the highest concentration of drug in the theranostic nanoparticles showed mild hemolysis which is less than <5% and under acceptable limits as per the ASTM standards E254-08. The reference values for the hemolysis test shown in table 6.1. It can be concluded that the sample was mildly haemolytic due to the property of drug lenalidomide and iron oxide nanoparticles which are reported to cause hemolysis depending on the physicochemical characteristics like particle size, presence of polymeric coat and concentration (31, 32).

Table 6.1: Reference values for the hemolysis as per ASTM E254-08 guidelines.

% Hemolysis	Inference
<2%	Non haemolytic sample
2-5%	Mildly haemolytic sample
>5%	Haemolytic sample

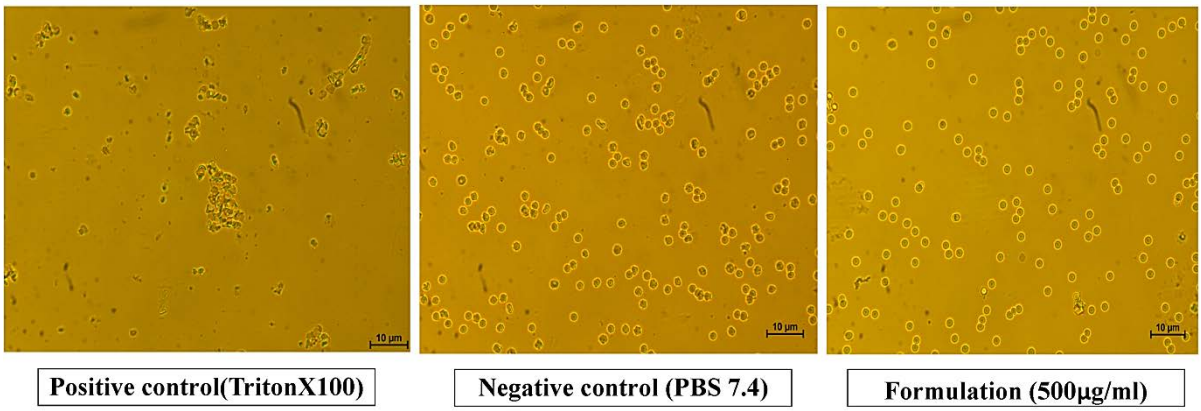

Figure 6.11: RBC morphology after treatment with positive control, negative control and formulation of theranostic nanoparticles.

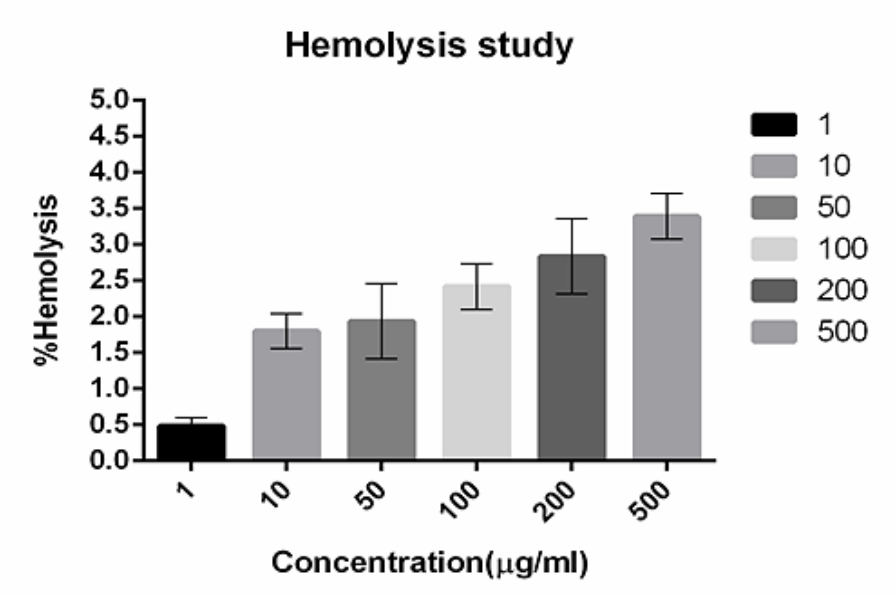

Figure 6.12: Results of haemolytic toxicity study for formulation (n=3).

6.10. References.

1. Kumar P, Nagarajan A, Uchil PD. Analysis of cell viability by the MTT assay. Cold Spring Harbor Protocols. 2018;2018(6):pdb. prot095505.
2. Mondal S, Manivasagan P, Bharathiraja S, Santha Moorthy M, Nguyen VT, Kim HH, et al. Hydroxyapatite coated iron oxide nanoparticles: a promising nanomaterial for magnetic hyperthermia cancer treatment. Nanomaterials. 2017;7(12):426.
3. Liu X, Du C, Li H, Jiang T, Luo Z, Pang Z, et al. Engineered superparamagnetic iron oxide nanoparticles (SPIONs) for dual-modality imaging of intracranial glioblastoma via EGFRvIII targeting. Beilstein journal of nanotechnology. 2019;10(1):1860-72.
4. Ibiyeye KM, Nordin N, Ajat M, Zuki ABZ. Ultrastructural changes and antitumor effects of doxorubicin/thymoquinone-loaded CaCO3 nanoparticles on breast cancer cell line. Frontiers in oncology. 2019;9:599.
5. Lu VM, Crawshay-Williams F, White B, Elliot A, Hill MA, Townley HE. Cytotoxicity, dose-enhancement and radiosensitization of glioblastoma cells with rare earth nanoparticles. Artificial cells, nanomedicine, and biotechnology. 2019;47(1):132-43.
6. Pinheiro PC, Daniel-da-Silva AL, Tavares DS, Calatayud MP, Goya GF, Trindade T. Fluorescent magnetic bioprobes by surface modification of magnetite nanoparticles. Materials. 2013;6(8):3213-25.
7. Shevtsov M, Nikolaev B, Marchenko Y, Yakovleva L, Skvortsov N, Mazur A, et al. Targeting experimental orthotopic glioblastoma with chitosan-based superparamagnetic iron oxide nanoparticles (CS-DX-SPIONs). Int J Nanomedicine. 2018;13:1471-82. PubMed PMID: 29559776. eng.
8. Shen Z, Chen T, Ma X, Ren W, Zhou Z, Zhu G, et al. Multifunctional Theranostic Nanoparticles Based on Exceedingly Small Magnetic Iron Oxide Nanoparticles for T1-Weighted Magnetic Resonance Imaging and Chemotherapy. ACS Nano. 2017 2017/11/28;11(11):10992-1004.
9. Pezzini I, Marino A, Del Turco S, Nesti C, Doccini S, Cappello V, et al. Cerium oxide nanoparticles: the regenerative redox machine in bioenergetic imbalance. Nanomedicine. 2017;12(4):403-16.
10. Deweirdt J, Quignard J-F, Lacomme S, Gontier E, Mornet S, Savineau J-P, et al. In vitro study of carbon black nanoparticles on human pulmonary artery endothelial cells: effects on calcium signaling and mitochondrial alterations. Archives of toxicology. 2020;94:2331-48.
11. Mortimer M, Kasemets K, Kahru A. Toxicity of ZnO and CuO nanoparticles to ciliated protozoa Tetrahymena thermophila. Toxicology. 2010;269(2-3):182-9.
12. Prajapati JB, Patel GC. Nose to brain delivery of Rotigotine loaded solid lipid nanoparticles: Quality by Design based optimization and characterization. Journal of Drug Delivery Science and Technology. 2021 2021/01/27/:102377.
13. Bruinsmann FA, Pigana S, Aguirre T, Dadalt Souto G, Garrastazu Pereira G, Bianchera A, et al. Chitosan-Coated Nanoparticles: Effect of Chitosan Molecular Weight on Nasal Transmucosal Delivery. Pharmaceutics. 2019;11(2):86. PubMed PMID: doi:10.3390/pharmaceutics11020086.
14. Feng Q, Liu Y, Huang J, Chen K, Huang J, Xiao K. Uptake, distribution, clearance, and toxicity of iron oxide nanoparticles with different sizes and coatings. Scientific reports. 2018;8(1):1-13.
15. da Costa LS, Khan LU, Franqui LS, de Souza Delite F, Muraca D, Martinez DST, et al. Hybrid magneto-luminescent iron oxide nanocubes functionalized with europium complexes: synthesis, hemolytic properties and protein corona formation. Journal of Materials Chemistry B. 2021.
16. Präbst K, Engelhardt H, Ringgeler S, Hübner H. Basic colorimetric proliferation assays: MTT, WST, and resazurin. Cell viability assays: Springer; 2017. p. 1-17.
17. Bharathi D, Preethi S, Abarna K, Nithyasri M, Kishore P, Deepika K. Bio-inspired synthesis of flower shaped iron oxide nanoparticles (FeONPs) using phytochemicals of Solanum lycopersicum leaf extract for biomedical applications. Biocatalysis and Agricultural Biotechnology. 2020;27:101698.

18. Pijuan J, Barceló C, Moreno DF, Maiques O, Sisó P, Marti RM, et al. In vitro cell migration, invasion, and adhesion assays: from cell imaging to data analysis. Frontiers in cell and developmental biology. 2019;7:107.
19. Matuszak J, Lutz B, Sekita A, Zaloga J, Alexiou C, Lyer S, et al. Drug delivery to atherosclerotic plaques using superparamagnetic iron oxide nanoparticles. Int J Nanomedicine. 2018;13:8443.
20. Pernal S, Wu VM, Uskoković V. Hydroxyapatite as a vehicle for the selective effect of superparamagnetic iron oxide nanoparticles against human glioblastoma cells. ACS applied materials & interfaces. 2017;9(45):39283-302.
21. Costantino L, Tosi G, Ruozi B, Bondioli L, Vandelli MA, Forni F. Chapter 3 - Colloidal systems for CNS drug delivery. In: Sharma HS, editor. Progress in Brain Research. 180: Elsevier; 2009. p. 35-69.
22. Battogtokh G, Cho Y-Y, Lee JY, Lee HS, Kang HC. Mitochondrial-Targeting Anticancer Agent Conjugates and Nanocarrier Systems for Cancer Treatment. Frontiers in Pharmacology. 2018 2018-August-17;9(922). English.
23. Ordys BB, Launay S, Deighton RF, McCulloch J, Whittle IR. The role of mitochondria in glioma pathophysiology. Molecular neurobiology. 2010;42(1):64-75.
24. Ke S, Zhou T, Yang P, Wang Y, Zhang P, Chen K, et al. Gold nanoparticles enhance TRAIL sensitivity through Drp1-mediated apoptotic and autophagic mitochondrial fission in NSCLC cells. Int J Nanomedicine. 2017;12:2531-51. PubMed PMID: 28408823. eng.
25. Gutiérrez-Carcedo P, Navalón S, Simó R, Setoain X, Aparicio-Gómez C, Abasolo I, et al. Alteration of the Mitochondrial Effects of Ceria Nanoparticles by Gold: An Approach for the Mitochondrial Modulation of Cells Based on Nanomedicine. Nanomaterials. 2020;10(4):744.
26. Zorova LD, Popkov VA, Plotnikov EY, Silachev DN, Pevzner IB, Jankauskas SS, et al. Mitochondrial membrane potential. Analytical biochemistry. 2018 Jul 1;552:50-9. PubMed PMID: 28711444. Pubmed Central PMCID: PMC5792320. Epub 2017/07/18. eng.
27. Ducray AD, Felser A, Zielinski J, Bittner A, Bürgi JV, Nuoffer J-M, et al. Effects of silica nanoparticle exposure on mitochondrial function during neuronal differentiation. Journal of nanobiotechnology. 2017;15(1):1-14.
28. Bendale Y, Bendale V, Paul S. Evaluation of cytotoxic activity of platinum nanoparticles against normal and cancer cells and its anticancer potential through induction of apoptosis. Integrative medicine research. 2017;6(2):141-8.
29. Pan L, Zhou J, Ju F, Zhu H. Intranasal delivery of α-asarone to the brain with lactoferrin-modified mPEG-PLA nanoparticles prepared by premix membrane emulsification. Drug delivery and translational research. 2018;8(1):83-96.
30. Tzeyung AS, Md S, Bhattamisra SK, Madheswaran T, Alhakamy NA, Aldawsari HM, et al. Fabrication, optimization, and evaluation of rotigotine-loaded chitosan nanoparticles for nose-to-brain delivery. Pharmaceutics. 2019;11(1):26.
31. Mesdaghinia A, Pourpak Z, Naddafi K, Nodehi RN, Alizadeh Z, Rezaei S, et al. An in vitro method to evaluate hemolysis of human red blood cells (RBCs) treated by airborne particulate matter (PM10). MethodsX. 2019;6:156-61.
32. Easo SL, Mohanan P. In vitro hematological and in vivo immunotoxicity assessment of dextran stabilized iron oxide nanoparticles. Colloids and Surfaces B: Biointerfaces. 2015;134:122-30.